

Phase Crossover induced by Dynamical Many Body Localization in Periodically Driven Long-Range Spin Systems

Mahbub Rahaman,¹ Takashi Mori,² and Analabha Roy¹

¹Department of Physics, The University of Burdwan, Golapbag, Bardhaman - 713 104, India

²RIKEN CEMS, 2-1 Hirosawa, Wako, Saitama, 351-0198, Japan

Dynamical many-body freezing occurs in periodic transverse field-driven integrable quantum spin systems. Under resonance conditions, quantum dynamics causes practically infinite hysteresis in the drive response, maintaining its starting value. We extended this to non-integrable many body systems by reducing the Hamiltonian symmetries through a power-law dependence in spin exchange energy, $J_{ij} = 1/|i - j|^\beta$. The dynamics of the integrable short-range Transverse Field Ising Model (TFIM) and non-integrable long-range Lipkin Meshkov-Glick (LMG) models were investigated. In the LMG, the resonance conditions in the driving field suppresses the heating postulated by the *Eigenstate Thermalization Hypothesis* (ETH) by inducing *Dynamical Many Body Localization*, or DMBL. This is in contrast to Many Body Localization (MBL), which requires disorder to suppress ETH. DMBL has been validated by the Inverse Participation Ratio (IPR) of the quasi-stationary Floquet modes. While TFIM has IPR localization for all drive parameters, the LMG exhibits high-frequency localization only at the resonances. IPR localization in the LMG deteriorates with an inverse system size law at lower frequencies, which indicates heating to infinite temperature. Furthermore, adiabatically increasing frequency and amplitude from low values raises the Floquet state IPR in the LMG from nearly zero to unity, indicating a phase crossover. This occurrence enables a future technique to construct an MBL engine in clean systems that can be cycled by adjusting drive parameters only.

Keywords: Dynamical localization, Thermalization, Phase Crossover

Periodically driven Quantum Many Body Systems can experience Dynamical Freezing (DMF) when dynamical hysteresis stops observables from reaching their diagonal averaged values and thermalizing to infinite temperature [1–3]. Under certain resonance conditions in the drive parameters, DMF can cause the response to ‘freeze’ completely to its initial value at all times. This arises as a consequence of additional approximate symmetries that occur at resonance. DMF has been demonstrated via the Rotating Wave Approximation (RWA) in the driven TFIM with nearest neighbour interactions [4] and is shown to be protected when translational invariance is explicitly broken (say, by disorder) [5, 6].

The utilization of Floquet theory simplifies the analysis of time-periodic systems. For closed quantum systems governed by the time-dependent Schrödinger equation, the *Floquet Hamiltonian* allows for a mapping of the time-dependent dynamics into the dynamics of a time-independent effective Hamiltonian, provided the system is strobed at integer multiples of the time period of the drive. The time independent eigenstates of the effective Hamiltonian correspond to quasi-stationary *Floquet Modes* of the original Hamiltonian. The temporal progression of the system comes from phase coefficients that capture the dynamics [7, 8].

Any sufficiently complex non-integrable Many Body System is expected to thermalize according to the Eigenstate Thermalization Hypothesis (ETH) despite

the fact that closed quantum dynamics preserves the memory of the initial state of the system. This arises due to the properties of the matrix elements of observables in typical states[9]. The ETH can be readily adapted to time-periodic systems using Floquet theory (the Floquet-ETH, or FETH). Nonetheless, the conditions for ETH to hold are not particularly strong, and the density matrix of the system can fail to approach one that is described by a thermal expression. In such cases, the system is said to undergo *Many Body Localization* (MBL)[10]. This phenomenon is stable against local perturbations, and constitutes an exotic state of matter with far-reaching implications in theoretical physics, as well as in practical applications[11].

The addition of disorder has been identified as a crucial component in the onset of MBL. In that case, thermalization is prevented by disorder-induced localization. An alternative approach to realizing MBL in clean many-body system involves *Floquet Engineering*, where a time-periodic drive is introduced, and the drive parameters tuned so as to introduce a clustering of quasistationary energies in a manner similar to localization[9].

In this article, we propose that additional approximate symmetries can be Floquet-engineered in quantum many body systems with lower symmetry than the TFIM, such as those with long-range interactions. This results in both DMF and MBL occurring simultaneously at resonant values of the drive parameters, and complete thermal behaviour at other values. This

None the
al-
ter-
na-
tive
ap-
proach-
es to
MBL
in
disorder-
free
sys-
tems
by
peri-
od-
driv-
ing

68 phenomenon is distinct from DMF in the TFIM, since 120
 69 clean TFIM systems, being integrable, never thermal-
 70 ize.

71 To demonstrate the onset of MBL, we investigate 121
 72 the driven Lipkin-Meshkov-Glick (LMG) model, a long-
 73 range system that is a special case of the more general
 74 Curie-Weiss model, wherein the nearest-neighbour ex-
 75 change in the TFIM is extended to longer ranges with
 76 a power law dependence, $J_{ij} \sim 1/|i - j|^\beta$ [12-14].
 77 Setting $\beta = \infty$ recovers the TFIM, and setting $\beta = 0$
 78 yields the LMG model. We have recovered the onset
 79 of DMF in this system and have supported our result
 80 with numerical simulations.

81 In addition, we compare the degree of localization 122
 82 of the quasi-stationary Floquet modes in both limits of
 83 β . In order to do so, we look at the Inverse Partici-
 84 pation Ratio (IPR) of the Floquet modes in the repre-
 85 sentation given by the eigenstates of the symmetry-
 86 breaking field. The IPR, closely related to the concept
 87 of quantum purity, is defined as the formal sum of the
 88 square of the density in some physically meaningful
 89 space or representation. A high IPR of a stationary
 90 state denotes low participation in most of the repre-
 91 sentation, and a low IPR distributes participation uni-
 92 formly across the representation, leading to ergodic
 93 dynamics[15]. Thus, IPR [16] is a useful tool for wit-
 94 nessing MBL of a quantum system. For an MBL sys-
 95 tem, the IPR is unity, and it scales inversely with the
 96 system size when it is thermally distributed [17].

97 In the first section of this paper, we present all es-
 98 sential theoretical frameworks. Our results for the
 99 LMG model are presented next in section II. In that
 100 section, we have used the Rotating Wave Approx-
 101 imation (RWA) [18], where only the slowest rotating
 102 terms in the Fourier expansion of the Hamiltonian in
 103 a frame co-rotating with the symmetry breaking drive
 104 field are retained. In addition, we have the obtained
 105 analytical expressions for the Floquet modes and their
 106 IPR. They are used to probe the system dynamics in
 107 the high and low-frequency domains at both limits of
 108 β . In section III we have used phase space plots to
 109 contrast the low and high frequency limits of the LMG
 110 model in the thermodynamic limit by mapping it to an
 111 equivalent classical Hamiltonian system. Finally, in
 112 section IV, we have looked at numerical computations
 113 of the IPR of the Floquet modes for different values of
 114 the drive parameters, well beyond those that allow for
 115 the RWA. We observed that, if the system is driven by
 116 an adiabatically increasing drive frequency from low
 117 to high limit while remaining in the resonance region,
 118 a sharp crossover from a thermal to an MBL phase
 119 occurs. We conclude with discussions and outlook.

I. BACKGROUND

121 The Eigenstate Thermalization Hypothesis (ETH) is
 122 a series of conjectures that allows for the thermaliza-
 123 tion of an isolated quantum many body system. The
 124 state of the system, $|\psi(t)\rangle$, evolves according to the
 125 Schrödinger equation $\hat{H}|\psi(t)\rangle = i\frac{\partial}{\partial t}|\psi\rangle$. The Hamilto-
 126 nian \hat{H} is assumed to be *non-integrable*, in that it lacks
 127 an extensive number of *local* additive conserved quan-
 128 tities, that is to say, there are no set of observables
 129 \hat{O}_s such that $\hat{H} = \sum_s \hat{O}_s$ for any extensive index s .
 130 Here, the \hat{O}_s constitute an arbitrary CSCO (complete
 131 set of commuting observables) that are *local*, having
 132 sub-extensive support in the system size. In addition,
 133 we postulate the existence of an equivalent Hamilto-
 134 nian \hat{H}_{eq} for every Hamiltonian \hat{H} as well as an "equi-
 135 librium" value A_{eq} for every observable \hat{A} , such that

$$A_{eq}(E) \equiv \frac{\text{Tr}(\hat{A}e^{-\beta\hat{H}_{eq}})}{\text{Tr}(e^{-\beta\hat{H}_{eq}})}. \quad (1)$$

136 where $E = \langle\psi(t)|\hat{H}|\psi(t)\rangle$ is the conserved energy of
 137 the system, and $\beta = 1/(k_B T)$ is the inverse tempera-
 138 ture, H_{eq} is an effective Hamiltonian that captures the
 139 long-time average dynamics of the system, and k_B is
 140 the Boltzmann constant.

To put it simply, ETH proposes that this many-
 body Hamiltonian undergoes thermalization as seen
 in the *long-time averages* of observables, with the
 eigenstates bearing resemblance to thermal states.
 The aforementioned hypothesis serves as a valuable
 instrument for comprehending the conduct of stim-
 ulated quantum systems and their correlation with
 thermal equilibrium. This assertion can be justified
 by examining the expectation value of an observable
 \hat{A} as it evolves under the Schrödinger equation. To
 see this, we first expand the state of the system $|\psi(t)\rangle$
 as:

$$|\psi(t)\rangle = \sum_m c_m(t) |m(0)\rangle,$$

141 where $|m(0)\rangle$ represents the eigenstates of $\hat{H}(0)$ with
 142 energy E_m . The coefficients $c_m(t)$ describe the time-
 143 dependent amplitude of the expansion. Plugging
 144 these expansions into the expression for the expec-
 145 tation value, we obtain the long-time average of the
 146 expectation value [19]:

$$\overline{\langle \hat{A}(t) \rangle} = \sum_{m,k} \overline{c_m^*(t)c_k(t)} \langle m(0)|\hat{A}|k(0)\rangle, \quad (2)$$

147 where the overline indicates the following operation
 148 for any time-dependent quantity $\mathcal{O}(t)$,

$$\overline{\mathcal{O}} \equiv \lim_{T \rightarrow \infty} \frac{1}{T} \int_0^T dt \mathcal{O}(t). \quad (3)$$

Had the system been integrable, the large number of conserved quantities would restrict mixing between the states during unitary evolution. In the non-integrable case, the system explores the entire Hilbert space spanned by eigenstates with eigenvalues close to E more-or-less uniformly. In that case, the matrix elements $\langle m(0)|\hat{A}|k(0)\rangle$ are said to satisfy the Srednicki ansatz [20, 21]:

$$\langle m(0)|\hat{A}|k(0)\rangle \approx A_{eq} \left(\frac{E_m + E_k}{2} \right) \delta_{mk} + e^{-\frac{1}{2}S\left(\frac{E_m+E_k}{2}\right)} f\left(\frac{E_m + E_k}{2}, E_m - E_k\right) R_{mk}. \quad (4)$$

Here, S is the thermodynamic entropy and R_{mk} are elements of a random matrix with vanishing mean and unit variance. What this means for the ensuing dynamics is that the system explores the accessible Hilbert space uniformly, and the matrix elements $\langle m(0)|\hat{A}(t)|k(0)\rangle$ become indistinguishable for most pairs of m and k . Applying this ansatz and taking the thermodynamic limit by ignoring terms $\mathcal{O}(e^{-S/2})$, the expression for the expectation value becomes:

$$\overline{\langle \hat{A}(t) \rangle} \approx \sum_m \overline{|c_m(t)|^2} A_{eq} \left(\frac{E_m + E_k}{2} \right) \approx A_{eq}(E) \sum_m \overline{|c_m(t)|^2} = A_{eq}(E),$$

where, in the last step, we utilized the fact that A_{eq} is a smooth function, and that the states with energies far from E have $|c_m(t)|^2 \approx 0$. Therefore, in the limit of large systems the expectation value of an observable \hat{A} is approximately equal to the thermal expectation value A_{eq} . This is the essence of the ETH, which suggests that individual eigenstates of a quantum system can be described by statistical mechanics in the long-time limit.

We now generalize the ETH to non-integrable many-body systems that are closed, but not isolated. In that case, it is possible to impart a periodic time-dependence on the Hamiltonian while still ensuring unitary evolution. If the time period of the drive is T , and the corresponding drive frequency $\omega \equiv 2\pi/T$, the Floquet theorem states that the solutions to the Schrödinger equation can be written as $|\psi(t)\rangle = e^{-i\epsilon t/\hbar} |\phi(t)\rangle$, where the $|\phi(t)\rangle$ are T -periodic states called *Floquet Modes*, the corresponding $\epsilon \in \mathbb{R}$, are called *quasienergies*. Quasienergy values are not unique, and can be made to be bounded within a Floquet photon, viz. a range $[-\omega/2, \omega/2]$ [22, 23]. As a consequence, the unitary evolution operator can be split into two parts as follows [24].

$$U(t) = e^{-i\hat{K}_F(t)} e^{-i\hat{H}_F t}. \quad (5)$$

Here, the micromotion operator $\hat{K}_F(t)$ is time-periodic in T , with $\hat{K}_F(0) = 0$, and the Floquet Hamiltonian $\hat{H}_F = \hat{H}(t) - i\frac{\partial}{\partial t}\Big|_{t=T}$. Thus, if the system is strobed at integer multiples of T only, then the unitary evolution matches that of a time independent Hamiltonian H_F . This can capture most of the exact dynamics at large frequencies.

In such systems, the Floquet Eigenstate Thermalization Hypothesis (FETH) posits that, subject to specific conditions and in the context of a system of significant size, the Floquet modes themselves exhibit thermal state-like behavior, i.e., $\hat{H}_{eq} \approx \hat{H}_F$ in eqn 1. However, in contrast to the isolated systems, the loss of energy conservation allows for the mixing of all Floquet modes in the ensuing dynamics, not just those with quasienergies near E . Were this to actually happen in the ensuing dynamics, it can be reconciled with ETH [25] by ensuring that $\beta = 0$ in eq 1. In other words, the nonequilibrium steady state of the system tends to an infinite temperature, maximum entropy density matrix.

However, drive parameters like amplitude, frequency, and duty-cycle strongly affect the structure of the Floquet modes $|\phi\rangle$. Thus, they can be engineered to prevent the kind of full mixing that would lead to infinite temperatures, manifesting suppression of thermalization dynamically. Thus, this type of *Floquet Engineering* can produce *Dynamical Many Body Localization* (DMLB), where the system fails to reach thermal equilibrium and remains localised, possibly near its initial state, even at large times. This paradigm seems similar to standard Many-Body Localization [26, 27], where disorder, locality, and integrability can cause athermalism via breakdown in the Srednicki ansatz. However, DMLB is a purely dynamical phenomenon, and thus can occur regardless of disorder, locality of observables, or system integrability, all of which have been studied for MBL onset [28–30].

Integrable Many Body systems do not exhibit thermalization. When subjected to time-periodic drives, Floquet engineering allows for the introduction of additional approximate conserved quantities that dynamically suppress the evolution of certain observables by hysteresis. This type of *freezing* of response has been shown in integrable systems [6]. A paradigmatic example is the driven Transverse Field Ising model (TFIM) in one dimension [31]. The Hamiltonian

is given by

$$\hat{H}(t) = \hat{H}_0 + h_z(t) \hat{H}_1 \quad (6)$$

$$\hat{H}_0 = -\frac{1}{2} \sum_{i=1}^N \sigma_i^x \sigma_{i+1}^x \quad (7)$$

$$\hat{H}_1 = -\frac{1}{2} \sum_{i=1}^N \sigma_i^z. \quad (8)$$

Here, the undriven Hamiltonian \hat{H}_0 consists of nearest-neighbour interactions between N number of spin-1/2 particles on a one-dimensional spin network. The transverse field is denoted by \hat{H}_1 , and is being varied by a time-periodic and harmonic signal $h_z(t) = h_0 + h \cos \omega t$, yielding a time period $T = 2\pi/\omega$ with amplitude h , drive frequency ω , and d.c. field h_0 . This Hamiltonian can be readily transformed into a spinless pseudo-fermionic system via the Jordan-Wigner transformation [4]. When written in momentum space spanned by spinors $\psi_k = (c_{-k}, c_k^\dagger)^T$ of fermions at momentum k created (annihilated) by operators c_k^\dagger (c_k), the effective Hamiltonian

$$H(t) = \sum_{(k,-k)-\text{pairs}} \psi_k^\dagger \left[\left(f_k - h_z(t) \right) \tau_z + \tau_x \Delta_k \right] \psi_k \quad (9)$$

with $f_k = J \cos k$, $\Delta_k = J \sin k$, τ_{xyz} are the three Pauli Matrices, and the sum is over distinct $(k, -k)$ Cooper Pairs. We can transform our system to a frame that rotates with the time-varying symmetry-breaking field. This is achieved by the means of the unitary transformation operator

$$U(t) = \prod_k U_k(t) \quad (10)$$

$$U_k(t) = \exp \left\{ \left[\frac{i\hbar}{\omega} \sin \omega t \right] \tau_z \right\}.$$

The resulting transformed Hamiltonian $H'(t) = U^\dagger(t) H(t) U(t) - iU^\dagger(t) \partial_t U(t)$ simplifies to

$$H'(t) = \sum_{(k,-k)-\text{pairs}} \psi_k^\dagger \left[\tau_z f_k + \tau_x \cos(\eta \sin \omega t) + \tau_y \sin(\eta \sin \omega t) \right] \psi_k, \quad (11)$$

where we defined $\eta = 2h/\omega$. Using the Jacobi-Anger formula [32]

$$e^{i\eta \sin \omega t} = \sum_{n=-\infty}^{\infty} J_n(\eta) e^{in\omega t}, \quad (12)$$

where $J_n(\eta)$ are Bessel Functions, the transformed Hamiltonian simplifies to

$$H'(t) = \sum_{(k,-k)-\text{pairs}} \psi_k^\dagger \left\{ \tau_z f_k + 2\tau_x \Delta_k \sum_{n \geq 0} J_{2n}(\eta) \cos(2n\omega t) - 2\tau_y \Delta_k \sum_{n \geq 0} J_{2n+1}(\eta) \sin[(2n+1)\omega t] \right\} \psi_k, \quad (13)$$

In the frequency regime $\omega \gg f_k$, the long-time average $H^{RWA} \equiv \lim_{n \rightarrow \infty} \frac{1}{nT} \int_0^{nT} dt H'(t)$ can serve as a suitable approximation for $H'(t)$. This approximation, known as the *Rotated Wave Approximation* (RWA), eliminates the oscillating modes and results in an effective Hamiltonian that is independent of time.

$$H^{RWA} = \sum_{(k,-k)-\text{pairs}} \psi_k^\dagger \left[f_k \tau_z + 2J_0(\eta) \Delta_k \tau_x \right] \psi_k, \quad (14)$$

It is evident that by manipulating the drive parameters, specifically the amplitude denoted by h and the frequency denoted by ω , in a manner such that η is positioned on a root of $J_0(\eta)$, the fermion number can be conserved to a significant extent at this particular resonance. Consequently, it is feasible to exercise direct control over H^{RWA} , resulting in a comprehensive suppression of the dynamics of otherwise responsive observables.

This phenomenon is highly general in nature, and can be readily adapted to non-integrable systems. In such cases, freezing has the additional effect of inducing DMBL, suppressing thermalization to infinite temperatures. Numerical quantification of localization of a specific (quasi) stationary state in a physically significant representation can be achieved through the computation of the *Inverse Participation Ratio* (IPR). In the position representation, the IPR for a state $|\psi\rangle$ [33-36] is defined as

$$\phi_{IPR} \equiv \int dx |\langle x | \psi \rangle|^4$$

This definition can be generalized to the IPR of a state $|\phi\rangle$ in a representation given by complete orthonormal basis $|m\rangle$ as

$$\phi_{IPR} \equiv \sum_m |\langle m | \psi \rangle|^4. \quad (15)$$

The smallest value of the IPR corresponds to a fully delocalized state, $\psi(x) = 1/\sqrt{N}$ for a system of size N [36, 37]. Values of the IPR close to unity correspond to localized states [38]. For a periodically driven system, we look at the IPR of the quasi-stationary Floquet modes at $t = T$, where $t = 2\pi/\omega$ for drive frequency ω .

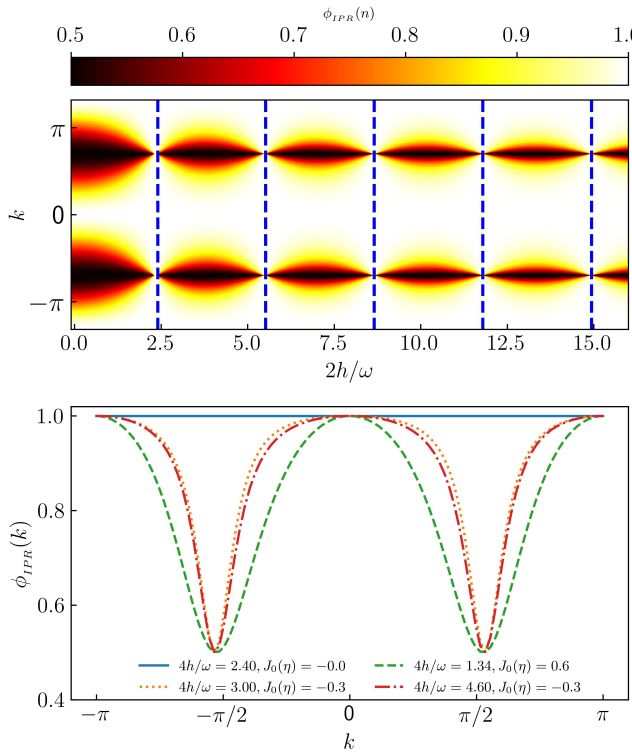


FIG. 1. Reduced IPR (defined in equation 16) for one of the two Floquet modes obtained from the exact dynamics of the TFIM for size $N = 100$ and $\omega = 90$ for the entire Brillouin zone (top panel, ordinate) and a few drive amplitudes (top panel, abscissa). The dashed lines (top panel) indicate the roots of $J_0(\eta)$. The bottom panel shows cross-sections for four different chosen amplitudes.

In the TFIM model, equation 14 indicates that, at resonance, when $J_0(\eta) = 0$, the Floquet modes are approximately given by the fermionic Fock states, which have a trivially unit IPR in the representation of the eigenmodes of the transverse field \hat{H}_1 in equation 6. Here, a particular Floquet mode can be decomposed into a direct product of cooper-pair states as $|\phi\rangle = \prod_{k,-k} |\phi_k^n\rangle$. In the RWA limit and at resonance, $|\phi_k^n\rangle$ has values of $|0\rangle, |k, -k\rangle$ for two values of $n = 0, 1$ respectively. We define the reduced IPR of $|\phi_k^n\rangle \forall k$ to be

$$\phi_{IPR}^{(n)}(k) = |\langle 0|\phi_k^n\rangle|^4 + |\langle +k, -k|\phi_k^n\rangle|^4, \quad (16)$$

where $n = 0, 1$. In the RWA limit and at resonance, this quantity is unity, indicating very low participation and the onset of freezing. Figure 1 shows results from numerically simulating the TFIM dynamics. The reduced IPR for a particular Floquet mode recovered by simulating the exact Schrödinger dynamics over a single time period of the drive, and plotted as a function of momentum k for different η 's. At resonance, when η lies at the root of the Bessel function $J_0(\eta)$,

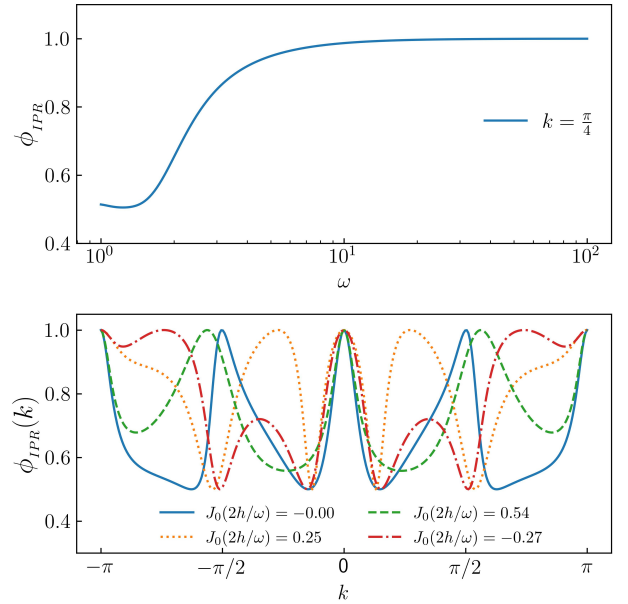


FIG. 2. Reduced IPR obtained by adiabatically increasing ω (top panel abscissa) for one the floquet mode obtained from equation 16 at the root of $J_0(\eta)$ for $N = 500$. IPR is ~ 0.5 (localized yet not fully freezing) upto $\omega \sim 2$, afterthat, smoothly increased to unity (fully localized and freezibg) at higher $\omega \geq 10$ (top panel, ordinate). At bottom panel cross-sections for four chosen amplitudes at $\omega = 2$ are plotted for a brillouin zone (abscissa) with corresponding reduced IPRs(ordinate).

the IPR is exactly unity for all momenta. Outside this resonance, the IPR is unity only for some momenta because the effective Hamiltonian is perfect diagonal at $k \in \{-\pi, 0, \pi\}$ as can be seen in the cross-sectional plots of figure 1. As we move away from the resonance point, IPR reduces from unity. However, as the TFIM is an integrable spin model, the IPR never drops to a value that is small enough to indicate thermalization. At low frequencies, RWA fails due to the unavailability of zero off-diagonal terms in the effective transformed Hamiltonian, as well as the absence of integrability breaking terms to counteract the off diagonal terms. Consequently, the IPR remains quite high (~ 0.5) even at the resonance point as can be seen figure 1. At low frequency, this is valid for all momentum and parameter η , see figure 2.

Because the dependence of observable expectations on the eigenstates is always fairly strong for integrable systems like the TFIM, such systems will never exhibit any kind of thermal behaviour unless integrability breaking terms (such as strong disorder) are included [6]. As a result, it is not physically meaningful to refer to the unit IPR region as "Many Body Localization", because the parameter space lacks a thermal-

ized region to contrast with this state. The type of Floquet Engineering described above, on the other hand, can be easily applied to a broad class of nonintegrable systems where FETH is expected to hold in certain regions. Long-range spin systems, in particular, where the exchange energies between far-off spins are taken into account in the model Hamiltonian, are good candidates because they are known to thermalize when driven with low frequencies [39].

II. LONG RANGE INTERACTIONS: THE LIPKIN MESHKOV GLICK MODEL:

The periodically driven Curie-Weiss model for N long-range spins is described by the Hamiltonian

$$\hat{H}(t) = \hat{H}_0 + [h \cos(\omega t) + h_0] \hat{H}_1. \quad (17)$$

Here, the undriven part \hat{H}_0 and the driven part \hat{H}_1 are, respectively,

$$\begin{aligned} \hat{H}_0 &= \frac{1}{2} \sum_{ij} J_{ij} \hat{\sigma}_i^z \hat{\sigma}_j^z, \\ \hat{H}_1 &= \sum_{i=1}^N \hat{\sigma}_i^x. \end{aligned} \quad (18)$$

The Heisenberg exchange energy of the bond between spins i and j is given by

$$J_{ij} = \frac{J_\alpha}{N^{1-\alpha}} \frac{1}{r_{ij}^\alpha}, \quad (19)$$

with r_{ij} representing the smallest graph distance between them. Putting $\alpha = 0$ yields the Lipkin Meshkov Glick (LMG) model with all-to-all interactions $J_{ij} = J_0/N \forall (i, j), i \neq j$. We choose to maintain the extensivity of the interaction energy by enforcing the condition

$$\frac{J_0}{N} \sum_{i \neq j} 1 = \frac{J_0}{N} \frac{N(N-1)}{2} = 1,$$

yielding the Kac-norm $J_0 = 2/(N-1)$. The Hamiltonian in equation 17 commutes with $P_{ij} \equiv \frac{1}{2}(1 + \vec{\sigma}_i \cdot \vec{\sigma}_j)$. In addition, it also commutes with the total angular momentum $S^2 = |\vec{S}|^2$, where $\vec{S} =$

$S^x \hat{x} + S^y \hat{y} + S^z \hat{z} \equiv \frac{1}{2} \sum_i \vec{\sigma}_i$. We now choose to populate the system in a state with $S^2 = \frac{N}{2} \left(\frac{N}{2} + 1 \right)$. In that case, the dynamics remains invariant in the $N+1$ -dimensional space spanned by the common eigen states of $P_{ij}, |S|^2$ and S_z ; the so-called *Totally Symmetric Subspace*, or TSS [40]. Let the eigenvalues of S^z in the TSS be s_n , and the eigen vectors be $|s_n\rangle$. Here, $s_n = -\frac{1}{2} + \frac{n}{N}$ and the index $n = 0(1)N$ has $N+1$ values. The dynamics is restricted to this invariant subspace, wherein the matrix elements of the Hamiltonian are given by

$$\begin{aligned} \langle s_i | \hat{H}_0 | s_j \rangle &= -\frac{4}{N-1} s_i^2 \delta_{ij}, \\ \langle s_i | \hat{H}_1 | s_j \rangle &= \left[\sqrt{\frac{N}{2} \left(\frac{N}{2} + 1 \right) - N s_i (N s_{i+1}) \delta_{i+1,j}} \right. \\ &\quad \left. + \sqrt{\frac{N}{2} \left(\frac{N}{2} + 1 \right) - N s_i (N s_{i-1}) \delta_{i-1,j}} \right] \end{aligned} \quad (20)$$

These allow for a numerical representation of the Hamiltonian in the TSS.

Next, we transform the Hamiltonian to the rotated frame given by the operator

$$\hat{U}(t) = \exp \left[i \frac{h}{\omega} \sin(\omega t) \hat{H}_1 \right]. \quad (21)$$

This is analogous to the rotation performed for the TFIM in eqns 10 and 11. Defining $\tau = \frac{h}{\omega} \sin \omega t$, we use the fact that $\hat{H}_1 = 2S^x$, as well as the following identity obtained by using the Baker-Campbell-Hausdorff formula,

$$e^{i2\tau \hat{S}^x} \hat{S}^z e^{-i2\tau \hat{S}^x} = \hat{S}^z \cos(2\tau) + \hat{S}^y \sin(2\tau), \quad (22)$$

to simplify the transformed Hamiltonian $\tilde{H}(t) = \hat{U}^\dagger(t) \hat{H}(t) \hat{U}(t) - \hat{U}^\dagger(t) \partial_t \hat{U}(t)$, yielding

$$\begin{aligned} \tilde{H}(t) &= -\frac{1}{N-1} \left[(S^z)^2 (1 + \cos 4\tau) + (S^y)^2 (1 - \cos 4\tau) \right. \\ &\quad \left. + \{S^y, S^z\} \sin 4\tau \right] - 2h_0 S^x. \end{aligned} \quad (23)$$

Next, we define $\eta \equiv 4h/\omega$ and use the Jacobi-Anger formula in eqn 12 to expand $\tilde{H}(t)$. Ignoring constant terms, this yields

$$\tilde{H}(t) \sim \frac{(\hat{S}^x)^2}{N-1} - 2h_0\hat{S}^x - \frac{J_0(\eta)}{N-1} \left[(\hat{S}^z)^2 - (\hat{S}^y)^2 \right] - \frac{2}{N-1} \sum_{k=1}^{\infty} J_{2k}(\eta) \left[(\hat{S}^z)^2 - (\hat{S}^y)^2 \right] \cos(2k\omega t) - \frac{2}{N-1} \sum_{k=1}^{\infty} J_{2k-1}(\eta) \{ \hat{S}^y, \hat{S}^z \} \sin[(2k-1)\omega t]. \quad (24)$$

If ω is large enough to smooth out the harmonic components, we obtain the RWA,

$$\tilde{H}(t) \approx \tilde{H}_{\text{RWA}} \equiv \frac{(\hat{S}^x)^2}{N-1} - 2h_0\hat{S}^x - \frac{J_0(\eta)}{N-1} \left[(\hat{S}^z)^2 - (\hat{S}^y)^2 \right]. \quad (25)$$

If the drive amplitude h is adjusted such that η lies at a root of $J_0(\eta)$ (the localization point), the RWA Hamiltonian is diagonal in the representation of the transverse field \hat{S}^x , yielding an IPR of unity in that representation, similar to the TFIM in the previous section. Note however, that if the DC transverse field h_0 is set to 0, then, at the localization point, the RWA Hamiltonian $\tilde{H}_{\text{RWA}} \sim (\hat{S}^x)^2$. The eigenvalues are two-fold degenerate. This produces infinitely many (Floquet) eigenmodes in the degenerate subspace whose IPRs may not always be unity in the S^x representation. The removal of this degeneracy necessitates the inclusion of the d.c. field h_0 . However, note that rational values of h_0 may add accidental degeneracies in \tilde{H}_{RWA} . To see this, note that, at a localization point, the eigenvalues of \tilde{H}_{RWA} in the TSS are given by

$$\text{Eigs}[\tilde{H}_{\text{RWA}}] = \frac{\left(\frac{N}{2} - m\right)^2}{N-1} - 2h_0 \left(\frac{N}{2} - m\right), \quad (26)$$

where the half-integer $-N/2 \leq m \leq N/2$ is the eigenvalue corresponding to a particular eigenstate $|m\rangle$ of the symmetry-breaking field \hat{S}^x . In order to ensure that no additional degeneracies occur, we have to set h_0 in such a way that no two energies accidentally coincide. If $N \gg 1$ (substantially large), then this condition can be readily met by assuring that $(1 - 2h_0)^{-1}$ is never an integer that is divisible by N . To ensure this in our numerical simulations, we have kept h_0 at a small irrational value.

The localization of the Floquet states at resonance is supported by exact numerical results, as can be seen in fig 3. Here, we show plots of the IPR of the Floquet modes $|\phi^n\rangle$ for $S^2 = (N/2)(N/2 + 1)$. The IPR in S^x representation is

$$\phi_{\text{IPR}}(n) = \sum_m |\langle m | \phi^n \rangle|^4. \quad (27)$$

These plots were obtained numerically by diagonalizing the propagator $U(t)$ at $t = T$, where $U(t)$ is defined

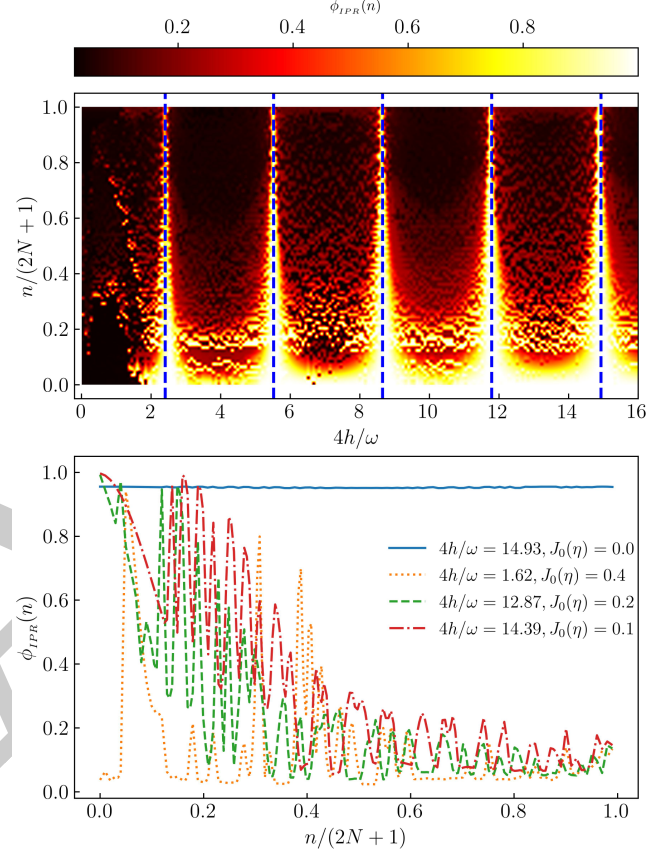


FIG. 3. IPR density plot for all possible Floquet modes (top panel ordinate) for different values of $\eta = 4h/\omega$ (top panel abscissa), deduced from equation 27 for exact LMG Hamiltonian for $N = 50$. Blue dashed lines are roots of $J_0(\eta)$. At bottom panel cross-section of IPR (ordinate) for four different η 's plotted for all possible floquet modes (bottom panel, abscissa) at $\omega = 90$. IPR founds to be \sim unity for all floquet modes at roots of J_0 .

in eqn 5. This propagator was obtained from simulations of the exact quantum dynamics using QuTiP, the Quantum Toolbox in Python [41]. We kept the frequency at a fairly large value $\omega = 90$ where we expect that RWA would be valid, and $N = \mathcal{O}(10^2)$. The density plot in the upper panel of fig 3 depicts the IPR of the Floquet states; the abscissa $\eta = 4h/\omega$ and the ordinate is $n/(2N+1)$, where $n \leq 2N$ is a nonnegative integer that indexes the Floquet states in increasing order of

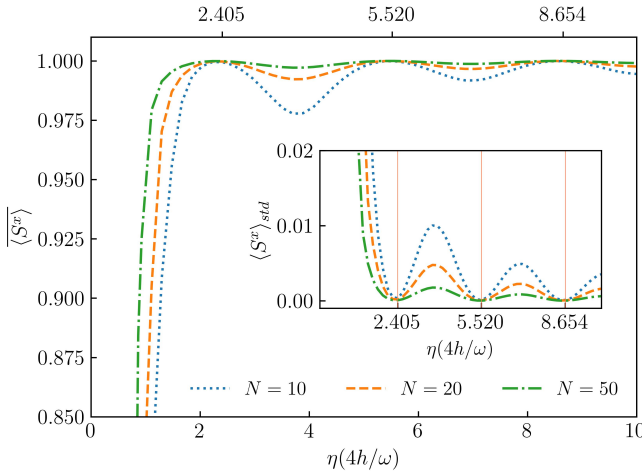


FIG. 4. Temporal average of $\langle \hat{S}^x \rangle$ (ordinate) for different η 's (abscissa) is plotted for $\sim 200T$ at higher ω for different $N=10,20,50$. $\langle \hat{S}^x \rangle$ is found to be unity at roots of $J_0(\eta)$. At points away from resonance points, $\langle \hat{S}^x \rangle$ falls below unity. The corresponding standard deviation $\langle \hat{S}^x \rangle_{std}$ supports the variation of $\langle \hat{S}^x \rangle$ (inset fig.). $\langle \hat{S}^x \rangle_{std}$ is ~ 0 describing a full freezing of the system at roots of $J_0(\eta)$ (red vertical solid lines).

³⁸⁴ m . The dashed vertical lines correspond to the roots
³⁸⁵ of $J_0(\eta)$. Comparing with the IPR of the TFIM in fig 1,
³⁸⁶ we can see a very similar patterns in the immediate
³⁸⁷ neighbourhood of the roots. Evidently, the IPR ap-
³⁸⁸ proaches a value of one for sufficiently large values of
³⁸⁹ the roots, strongly suggesting full DMBL. Deviations
³⁹⁰ occur at the smallest root of $J_0(\eta)$ (around $\eta = 2.405$)
³⁹¹ due to the contributions from higher order terms in
³⁹² eq 24. Thus, a higher root is favored for DMBL.

³⁹³ The bottom panel of fig 3 contains cross sections
³⁹⁴ of the full IPR plot for selected values of η as indi-
³⁹⁵ cated in the legend. When the drive amplitude h is
³⁹⁶ adjusted such that η is close to a root of $J_0(\eta)$, the Flo-
³⁹⁷ quet States are mixed, but not entirely thermal, since
³⁹⁸ the IPR does not fall to $\mathcal{O}(N^{-1})$, indicating that loca-
³⁹⁹ lization persists to some extent. However, the further
⁴⁰⁰ we are from the roots, the closer the IPR gets to one
⁴⁰¹ predicted by thermalization.

⁴⁰² Figure 4 shows plots of the long-time average (from
⁴⁰³ $t = 0 - 200T$) of the field amplitude $\langle \hat{S}^x \rangle$ as a function
⁴⁰⁴ of η . The system is started from the fully polarized
⁴⁰⁵ state $s_n = N/2$ in the TSS and the dynamics simulated.
⁴⁰⁶ The average is plotted for different values of ampli-
⁴⁰⁷ tude h , keeping the frequency fixed at a high value of
⁴⁰⁸ $\omega = 90$. It is clearly very close to unity at roots of $J_0(\eta)$
⁴⁰⁹ and falls at points away from it, indicating that S^x is
⁴¹⁰ approximately conserved at the localization points.

⁴¹¹ Small deviations do occur due to the role of higher

⁴¹² order terms in the rotated Hamiltonian in eq 23. This
⁴¹³ can be demonstrated quantitatively by comparing the
⁴¹⁴ IPR obtained from the exact dynamics simulation with
⁴¹⁵ that obtained from the dynamics of $\tilde{H}(t)$ in eq 23 after
⁴¹⁶ truncating the series at orders $k \geq 1$. This compari-
⁴¹⁷ son can be seen in fig 5. The IPR plots from the ex-
⁴¹⁸ act dynamics indicate that the first localization point,
⁴¹⁹ represented by the lowest root of $J_0(\eta)$, does not show
⁴²⁰ complete DMBL. However, DMBL is particularly con-
⁴²¹ spicuous at large roots. The IPRs of the Floquet states
⁴²² obtained from the RWA dynamics exhibit large devia-
⁴²³ tions from unity when away from the localization point
⁴²⁴ as evidenced by the green and red curves in the mid-
⁴²⁵ dle panel of fig 5. However, complete localization is
⁴²⁶ seen in the RWA dynamics at any localization point, in
⁴²⁷ contrast to the exact case in the top panel. Thus, it
⁴²⁸ is necessary to incorporate higher-order corrections
⁴²⁹ into the Rotating Wave Approximation (RWA) at lower
⁴³⁰ localization points. The application of the first-order
⁴³¹ correction to RWA in the lower panel of fig 5 results in
⁴³² a curve structure that is closer to that from the exact
⁴³³ dynamics.

III. PERSISTENCE OF DMBL IN THE CONTINUUM LIMIT

⁴³⁷ In the continuum limit, where $N \rightarrow \infty$, the dispari-
⁴³⁸ ty between neighboring values of s_i in equation 20
⁴³⁹ can be disregarded, and s_i can be mapped to a contin-
⁴⁴⁰ uum $q \in [-1/2, 1/2]$ [40]. We define the Hamiltonian
⁴⁴¹ per particle $h(t) \equiv \frac{\dot{H}(t)}{N}$, and a canonically conjugate
⁴⁴² co-ordinate $p \equiv \langle -i/N \frac{\partial}{\partial q} \rangle$. Then, in this limit, the
⁴⁴³ dynamics can be approximated by that of a classical
⁴⁴⁴ Hamiltonian [42]

$$h(t) = -2q^2 - [h \cos \omega t + h_0] \sqrt{1 - 4q^2} \cos p, \quad (28)$$

which yields the dynamical system

$$\begin{aligned} \frac{dq}{dt} &= \frac{\partial h}{\partial p} = h(t) \sqrt{1 - 4q^2} \sin p \\ \frac{dp}{dt} &= -\frac{\partial h}{\partial q} = 4q \left[1 - \frac{h(t) \cos p}{\sqrt{1 - 4q^2}} \right]. \end{aligned} \quad (29)$$

⁴⁴⁵ We have profiled simulations of the ensuing dynam-
⁴⁴⁶ ics with the *Poincaré surface of section* (PSOS) of the
⁴⁴⁷ full dynamics. Here, the (q, p) -phase space is strobed
⁴⁴⁸ at $t = nT$, and plotted for a large number of initial
⁴⁴⁹ conditions. The results are shown in the upper pan-
⁴⁵⁰ ells of fig 6 for a small value of $\omega = 2.5$ (left panel)
⁴⁵¹ and a large value $\omega = 90$ (right panel). In both cases,
⁴⁵² the value of h is chosen such that η lies on the first
⁴⁵³ root of $J_0(\eta)$. The onset of chaos for small drive fre-
⁴⁵⁴ quency indicates thermal behaviour for typical initial
⁴⁵⁵ conditions, with small islands of regularity for others.

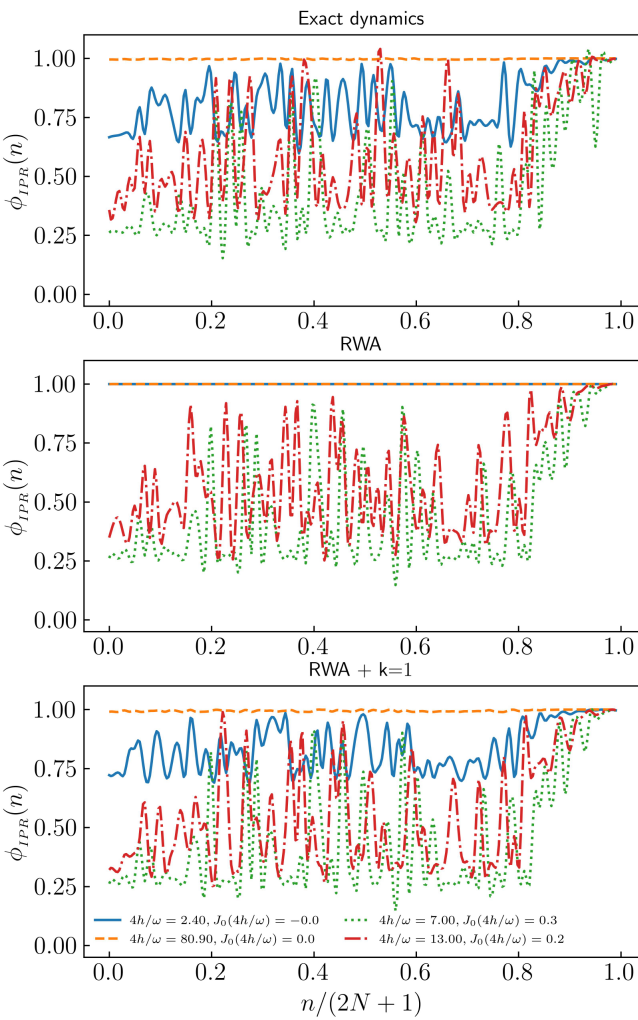


FIG. 5. The comparison between IPR for exact dynamics and RWA with corresponding correction orders. IPR is calculated for four different η 's and corresponding $J_0(\eta)$ values for colors, Blue: $\eta = 2.40, J_0(\eta) = 0.0$, dashed orange: $\eta = 80.9, J_0(\eta) = 0.0$, Green: $\eta = 7.0, J_0(\eta) = 0.3$, Red: $\eta = 13, J_0(\eta) = 0.2$. At low root of $J_0(\eta)$ IPR is not unity (Blue curve) where at higher root (orange dashed) it is unity while at points away from roots IPR are less than unity in the exact (top panel) plot. RWA does not matches with the exact plot. At all roots of $J_0(\eta)$ IPR is unity(middle panel). RWA with additional higher order terms exhibit similar system pattern(Bottom panel) with exact dynamics.

This is consistent with similar results for small frequencies reported in [39, 43]. However, at high frequency, the regular islands distinctly dominate over the chaos. The trajectories indicate that the conser-

vation of $\langle S^x \rangle \approx \sqrt{1 - 4q^2} \cos p$ [40] at high ω persists in the thermodynamic limit. That this is a signature of the underlying quantum dynamics can be readily seen in the quantum phase space representation of the Floquet Eigenstates for a large but finite N . These are shown in the corresponding lower panels of fig 6. Here, we have plotted the Spectral Average of the Husimi Q-functions of the acquired Floquet States in the TSS. Specifically, for a coherent state $|q, p\rangle$, the corresponding Spectral-Averaged Husimi distribution [44] is obtained by

$$H(q, p) \equiv \frac{1}{(2N+1)\pi} \sum_n \langle q, p | \phi^n \rangle \langle \phi^n | q, p \rangle \quad (30)$$

The quantum phase space retains signatures of the classical phase space dynamics when $N = 500$, indicating the onset of the persistence of S^x conservation that arises from the resonance condition at high frequencies.

IV. PHASE CROSSOVER FROM THERMAL TO DMBL

The analysis of the periodically driven LMG model reveals two distinct scenarios at low and high external drive frequencies. In the former case, thermalization in accordance with FETH is seen, whereas in the latter case, DMBL is induced. As a result, we hypothesize that a macroscopic change in phase occurs due to the influence of frequency.

To demonstrate this, we investigate the IPR of the Floquet mode with smallest quasienergy for numerous frequencies and system sizes, along with the associated drive amplitude h keeping the system at a localization point. The results are shown in fig 7. In the low-frequency range $\omega \in [1.0, 9.0]$, the IPR exhibits values well below unity. Moreover, the IPR gradually diminishes with increasing system size, following a system size inverse proportional trend, which confirms the participation distribution (as shown in the bottom panel). As the limit $N \rightarrow \infty$, the inverse participation ratio (IPR) tends towards zero, indicating a fully delocalized state. The plots reveal a gradual increase in the unity of IPR over a certain frequency range, specifically at $\omega \approx 5.0$. In addition, the rise does not cross with those for different values of N , suggesting the onset of a phase crossover [27, 45]. As the size of the system increases, the crossover region becomes smoother, rather than sharper.

We can also look at this crossover more clearly in the plots of the heating rate of the system, defined simply by the expectation value of the Hamiltonian, $\langle \hat{H}(t) \rangle$. We have carried out the numerical evaluation from the simulated dynamics over $t = 500T$. When the system is adequately described by FETH,

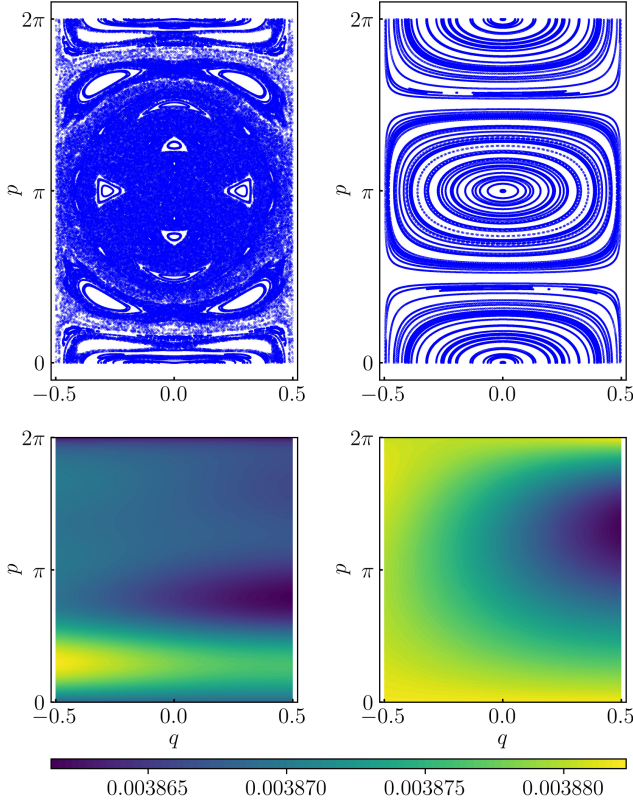


FIG. 6. Phase-space distributions at $\omega = 2.5$ (left panels) and $\omega = 90.0$ (right panels) for 100 initial conditions. At small ω , the classical PSOS, obtained from simulating the dynamics in eqns 29 (top left panel), shows chaotic behaviour, whereas at the higher ω , the onset of regular dynamics can be readily seen (top right panel). The bottom panels plot the corresponding Spectral-Averaged Husimi-Q function, obtained from the Floquet modes $|\phi^n\rangle$ using eqn 30. The $\omega = 2.5$ -case (bottom left panel) has a uniform distribution with less contrast in colour. This is consistent with the chaotic behaviour seen in the continuum limit. In the $\omega = 90$ -case (bottom right panel), the distribution has distinct colour contrasts, which is consistent with the regular dynamics pattern seen in the continuum limit.

the temporal fluctuations in the heating rate, defined by $\langle H \rangle_{std}^2 \equiv \overline{\langle \hat{H} \rangle^2} - \overline{\langle \hat{H} \rangle}^2$ (see eqn 3), are minimal in the thermodynamic limit, as the spread of states leads to a limited standard deviation[46]. Conversely, the onset of athermal behavior is indicated by nonzero fluctuations in time. If we set the initial state to the fully polarized state in the TSS (given by $|s_N\rangle$), then the onset of freezing, together with DMBL, will result in nearly infinite hysteresis in the ensuing dynamics, causing $|\psi\rangle(t) \approx |s_N\rangle \forall t$. From eqn 17, we can clearly see that this will lead to a linearly rising dependence on ω in

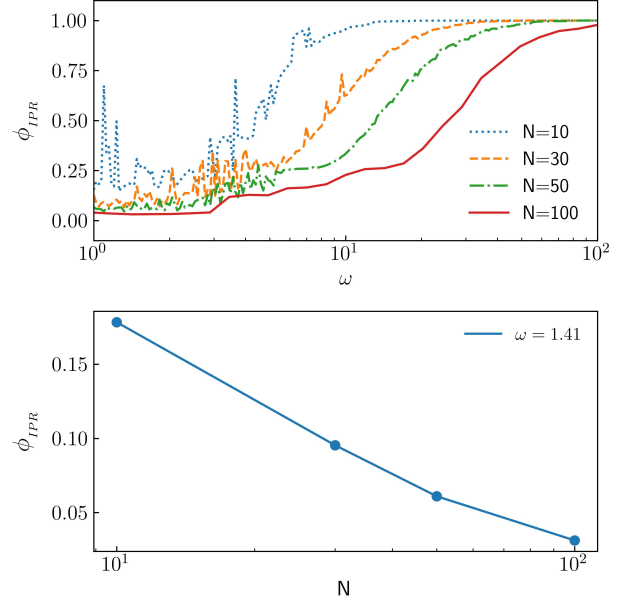


FIG. 7. IPR is plotted (top panel, ordinate) for a range of $\omega \in [1, 100]$ (top panel, abscissa) for four different $N = 10, 30, 50, 100$ at root of $J_0(\eta)$. At small ω upto $\omega \sim 10$ IPR founds to be very small and rises slowly upto unity (fully localized) at higher frequencies. At bottom panel IPR (ordinate) is plotted for different $N = 10, 30, 50, 100$ (bottom panel, abscissa) for a random small $\omega \sim 1$ at root of $J_0(\eta)$ from the values from top panel. IPR falls as proportional to inverse of N 's value which is a fully distributed state. The smooth rise in IPR defines a phase cross over (top panel) between a fully distributed thermal phase to a fully localized freezing phase.

⁵²² $\langle H \rangle_{std}$ as long as we stick to a localization point given
⁵²³ by a fixed h/ω . All these observations are corroborated
⁵²⁴ by the heating rate plots in figure 8.

V. CONCLUSION AND OUTLOOK

We have delved into the onset of freezing and phase cross-over in 1D spin systems driven by a time-periodic transverse field, contrasting the responses in the Transverse Field Ising Model (TFIM) with that of the long-range Lipkin-Meshkov-Glick Model (LMG). The parametrization of DMBL is based on the Inverse Participation Ratio (IPR) of the Floquet eigenstates. Our investigations compared the IPRs from both models numerically, and found the emergence of thermal behavior at low frequencies and freezing at high frequencies for the LMG model, the latter a direct consequence of the appearance of additional approximately conserved quantities.

⁵⁴⁰ Conclusion: Long-range spins exhibit strong localization in spin-coordinate space for the LMG model

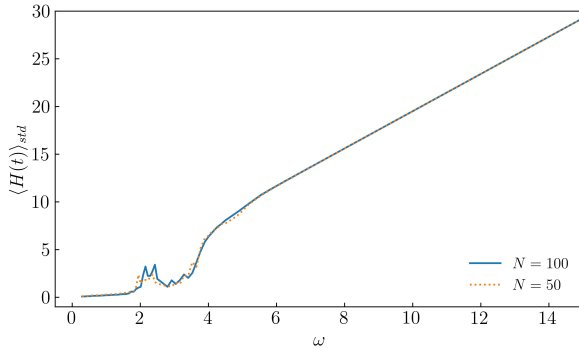


FIG. 8. The standard deviation of the heating rate, denoted by $\langle H \rangle_{std}$, calculated over a span of $t = 500T$ for two system sizes. Here, h is varied to keep $\eta = 4h/\omega$ at the first root of $J_0(\eta)$. A nonsingular rise has been identified at $\omega \approx 4.0$. $\langle H \rangle_{std}$ exhibits a diminutive magnitude below that value of ω , while a linear rise is observed at higher frequencies, consistent with freezing. A vanishingly small standard deviation for $\omega \ll 4.0$ indicates the presence of a thermal region, whereas a larger finite standard deviation suggests the existence of athermal behaviour. The small peaks observed at $\omega \in [2, 4]$ are finite-size effects that disappear in the thermodynamic limit.

when the drive frequency is $\omega \gg J$, where J represents the spin exchange energy. The localization of the LMG model occurs at specific resonance points of the drive frequency ω and amplitude h , at $J_0(4h/\omega) = 0$, $\omega \gg J$. This is apparently similar to the phenomenon of Dynamical Freezing (DMF) in the Transverse Field Ising Model (TFIM), where comparable localization at resonance points, determined by the roots of $J_0(2h/\omega)$ occurs due to the onset of an additional approximate conservation in the transverse field itself. However, a key difference is the thermal behaviour of the LMG model at low frequencies. Plots of the IPR for a range of frequencies along the resonance manifold exhibits a smooth increase in IPR yielding a

quantum phase-crossover from a thermal phase governed by the Floquet Eigenstate Thermalization Hypothesis (FETH) to a Dynamically Many-Body localized phase (DMBL). This crossover is absent in the TFIM, as can be readily seen in the significant magnitude of the inverse participation ratio (IPR) even at low frequencies. Thus, the suppression of thermalization through Dynamical Many Body Localization in long-range systems can be controlled via Floquet engineering, even in clean systems without any disorder.

Outlook:

We have demonstrated that periodically driven non-integrable long-range spin systems are an excellent tool for investigating disorder-free Many Body Localization, as can be readily seen via the IPR of its Floquet modes. We have compared the localization in the periodically driven LMG model with that in similarly driven short-range systems, and have observed a phase crossover from an FETH phase to a DMBL phase that arises due to Floquet Engineering.

There are several unexplored indicators of DMBL, such as entanglement entropy and level statistics ratio[10], which we defer to future studies. In addition, Halpern in 2019 proposed a quantum engine based on MBL[11] which works between strong localized and thermal phases of the system. In our proposed LMG model, tuning the system parameters by bringing them to the resonance points, then adiabatically cycling the frequency from the thermal region to the DMBL region, can achieve a similar engine without going through a phase transition.

Acknowledgement: One of the authors, MR would like to acknowledge The University of Burdwan for support via a state-funded fellowship, as well as for providing computational resources. AR acknowledges support from the University Grants Commission (UGC) of India, via BSR Startup Grant No. F.30-425/2018(BSR), as well as from the Science and Engineering Research Board (SERB) Core Research Grant No. CRG/2018/004002.

-
- [1] S. Bordia Pranjal, Lüschen Henrik, Nature Physics **13**, 460 (2017).
- [2] S. Sahoo, I. Schneider, and S. Eggert, Periodically driven many-body systems: A floquet density matrix renormalization group study (2019), arXiv:1906.00004 [cond-mat.str-el].
- [3] A. Das, Phys. Rev. B **82**, 172402 (2010).
- [4] G. B. Mbeng, A. Russomanno, and G. E. Santoro, The quantum ising chain for beginners (2020), arXiv:2009.09208 [quant-ph].
- [5] H. S. Yamada and K. S. Ikeda, Phys. Rev. E **105**, 054201 (2022).
- [6] A. Roy and A. Das, Phys. Rev. B **91**, 121106 (2015).
- [7] H. Li, B. Shapiro, and T. Kottos, Phys. Rev. B **98**, 121101 (2018).
- [8] A. Eckardt and E. Anisimovas, New Journal of Physics **17**, 093039 (2015).
- [9] L. Zhang, V. Khemani, and D. A. Huse, Phys. Rev. B **94**, 224202 (2016).
- [10] V. Khemani, A. Lazarides, R. Moessner, and S. L. Sondhi, Phys. Rev. Lett. **116**, 250401 (2016).
- [11] N. Yunger Halpern, C. D. White, S. Gopalakrishnan, and G. Refael, Phys. Rev. B **99**, 024203 (2019).
- [12] A. Campa, T. Dauxois, and S. Ruffo, Physics Reports **480**, 57 (2009).
- [13] E. R. S. Eisele, Theodor, Journal of Statistical Physics ,

- 622 161 (1988).
- 623 [14] A. Canning, Physica A: Statistical Mechanics and its
624 Applications **185**, 254 (1992).
- 625 [15] D. Vu, K. Huang, X. Li, and S. Das Sarma, Phys. Rev.
626 Lett. **128**, 146601 (2022).
- 627 [16] G. Misguich, V. Pasquier, and J.-M. Luck, Phys. Rev. B
628 **94**, 155110 (2016).
- 629 [17] M. Calixto and E. Romera, Journal of Statistical Me-
630 chanics: Theory and Experiment **2015**, P06029 (2015).
- 631 [18] K. Fujii, Journal of Modern Physics **8**, 2042 (2017).
- 632 [19] D. A. Abanin, E. Altman, I. Bloch, and M. Serbyn, Rev.
633 Mod. Phys. **91**, 021001 (2019).
- 634 [20] M. Srednicki, Phys. Rev. E **50**, 888 (1994).
- 635 [21] M. Srednicki, Journal of Physics A: Mathematical and
636 General **32**, 1163 (1999).
- 637 [22] M. Holthaus, Journal of Physics B: Atomic, Molecular
638 and Optical Physics **49**, 013001 (2015).
- 639 [23] M. Vogl, M. Rodriguez-Vega, and G. A. Fiete, Phys. Rev.
640 B **101**, 024303 (2020).
- 641 [24] M. Bukov, L. D'Alessio, and A. Polkovnikov, Advances in
642 Physics **64**, 139 (2015).
- 643 [25] L. D'Alessio and M. Rigol, Phys. Rev. X **4**, 041048
644 (2014).
- 645 [26] R. Yousefjani, S. Bose, and A. Bayat, Phys. Rev. Res. **5**,
646 013094 (2023).
- 647 [27] P. Sierant, M. Lewenstein, A. Scardicchio, and J. Za-
648 krzewski, Phys. Rev. B **107**, 115132 (2023).
- 649 [28] R. Yousefjani, S. Bose, and A. Bayat, Phys. Rev. Res. **5**,
650 013094 (2023).
- 651 [29] F. Alet and N. Laflorencie, Comptes Rendus Physique
652 **19**, 498 (2018).
- 653 [30] S. J. Garratt and S. Roy, Phys. Rev. B **106**, 054309
654 (2022).
- 655 [31] R. B. Stinchcombe, Journal of Physics C: Solid State
656 Physics **6**, 2459 (1973).
- 657 [32] F. E. H. George Arfken, Hans Weber, *Mathematical
658 Methods for Physicists*, 7th ed. (Academic Press).
- 659 [33] S. Mukherjee, A. Spracklen, D. Choudhury, N. Gold-
660 man, P. Öhberg, E. Andersson, and R. R. Thomson, New
661 Journal of Physics **17**, 115002 (2015).
- 662 [34] S.-H. Lin, B. Sbierski, F. Dorfner, C. Karrasch, and
663 F. Heidrich-Meisner, SciPost Phys. **4**, 002 (2018).
- 664 [35] N. C. Murphy, R. Wortis, and W. A. Atkinson, Phys. Rev.
665 B **83**, 184206 (2011).
- 666 [36] E. J. Torres-Herrera, I. Vallejo-Fabila, A. J. Martínez-
667 Mendoza, and L. F. Santos, Phys. Rev. E **102**, 062126
668 (2020).
- 669 [37] N. Trivedi and D. Heidarian, Progress of Theoretical
670 Physics Supplement **160**, 296 (2005).
- 671 [38] G. Misguich, V. Pasquier, and J.-M. Luck, Phys. Rev. B
672 **94**, 155110 (2016).
- 673 [39] A. Russomanno, R. Fazio, and G. E. Santoro, Euro-
674 physics Letters **110**, 37005 (2015).
- 675 [40] T. Mori, Journal of Physics A: Mathematical and Theo-
676 retical **52**, 054001 (2019).
- 677 [41] J. Johansson, P. Nation, and F. Nori, Computer Physics
678 Communications **184**, 1234.
- 679 [42] B. Sciolla and G. Biroli, Phys. Rev. Lett. **105**, 220401
680 (2010).
- 681 [43] R. A. Kidd, M. K. Olsen, and J. F. Corney, Phys. Rev. A
682 **100**, 013625 (2019).
- 683 [44] A. Bäcker, S. Fürstberger, and R. Schubert, Phys. Rev.
684 E **70**, 036204 (2004).
- 685 [45] S. Sachdev, *Quantum Phase Transitions*, 2nd ed. (Cam-
686 bridge University Press, Cambridge, 2011).
- 687 [46] P. Reimann, Journal of Statistical Mechanics: Theory
688 and Experiment **2021**, 103106 (2021).
- 689 [47] L. Reichl, *The Transition to Chaos: Conservative Clas-
690 sical and Quantum Systems*, Fundamental Theories of
691 Physics, Vol. 200 (Springer International Publishing).
- 692 [48] N. Srivatsa, R. Moessner, and A. E. Nielsen, Phys. Rev.
693 Lett. **125**, 240401.
- 694 [49] Quantum ising phase transition.
- 695 [50] B. Marcos, A. Gabrielli, and M. Joyce, Open Physics **10**,
696 676.
- 697 [51] A. Haldar and A. Das, Annalen der Physik **529**,
698 1600333.
- 699 [52] J. M. Deutsch, Phys. Rev. A **43**, 2046 ()�.
- 700 [53] E. W. Hobson, On the Second Mean-Value Theorem of
701 the Integral Calculus (1909).
- 702 [54] M. Rigol and M. Srednicki, Physical Review Letters
703 **108**, 10.1103/physrevlett.108.110601 (2012).
- 704 [55] J. M. Deutsch, IOP Publishing Ltd **81**, 296 ()�.
- 705 [56] R. Nandkishore and D. A. Huse, Annual Re-
view of Condensed Matter Physics **6**, 15 (2015),
706 https://doi.org/10.1146/annurev-conmatphys-031214-
707 014726.
- 708 [57] L. D'Alessio and A. Polkovnikov, **333**, 19.
- 709 [58] S. Notarnicola, F. Iemini, D. Rossini, R. Fazio, A. Silva,
710 and A. Russomanno, Phys. Rev. E **97**, 022202 (2018).
- 711 [59] S. Aditya and D. Sen, Dynamical localization and slow
712 thermalization in a class of disorder-free periodically
713 driven one-dimensional interacting systems (2023),
714 arXiv:2305.06056 [cond-mat.stat-mech].
- 715 [60] A. Lazarides, A. Das, and R. Moessner, Phys. Rev. Lett.
716 **115**, 030402 (2015).